EurJIC
European Journal of Inorganic Chemistry

Research Article
doi.org/10.1002/ejic.202100853

Chemistry Europe
European Chemical Societies Publishing

www.eurjic.org

Influencing the Dimensionality of Ni/Co-Bipyrazole-Based Coordination Frameworks through Anions and Thermal Activation

Ralph Freund,[a] Maryana Kraft,[a] and Dirk Volkmer*[a]

Thirteen Ni(II) and Co(II) coordination polymers based on the organic linker 1H,1′H-4,4′-bipyrazole (H_2BPZ) were synthesized and characterized using single crystal X-ray diffraction, namely $Ni(H_2BPZ)(acac)_2$ (**1**), $Ni(H_2BPZ)_2(H_2O)_2\cdot(NO_3)_2$ (**2**), $Ni_3(H_2BPZ)_6Cl_6\cdot(DMSO)_4$ (**3**), $Ni_8(H_2BPZ)_{16}Cl_{16}\cdot(DMSO)_6$ (**4**), $Ni(H_2BPZ)_2(H_2O)_6\cdot(ClO_3)_2(H_2O)_3$ (**5**), the isotypic structures $Ni(H_2BPZ)_2(CH_3SO_3)_2$ (**6**) and $Co(H_2BPZ)_2(CH_3SO_3)_2$ (**7**), $Co(H_2BPZ)_2(CF_3SO_3)_2$ (**8**), $Ni(H_2BPZ)_3\cdot(CF_3SO_3)_2$ (**9**), $Ni(H_2BPZ)_3\cdot(ClO_4)_2$ (**10**), $Co(H_2BPZ)_3\cdot(ClO_4)_2$ (**11**), $Ni(BPZ)\cdot(DMF)_{0.65}$ (**12**), and Ni(BPZ) (**13**). In order to study the structural correlations of 1D-3D, 2D-3D, and 3D-3D phase transitions the structures were investigated by means of thermal analysis. In addition, the role of charge-balancing anions with respect to their coordination strength on structure, framework dimension, and crystal properties is discussed in detail. This work exemplifies the function of anions as structure directing agents and how they, as well as thermal activation, can influence framework topology, dimensionality, and crystal size.

Introduction

Coordination Polymers (CPs) are a class of crystalline materials composed of metal ion containing secondary building units (SBUs) connected by bridging organic ligands,[1] which both can be chosen almost freely[2] and, moreover, changed retroactively[3]. While this alone results in a huge variety of structures, the framework topology and dimensionality can be further diversified by means of structure-directing and -stabilizing agents.[4,5] Besides a solvent and the organic linker, the synthesis of CPs involves a metal salt as source for metal cations. During the reaction different anionic and neutral species, including the solvent, compete with the organic linker for the "free" coordination sites at the metal centers.

The complex interplay of nucleation events in the reaction mixture, *i.e.*, polymorph selection and the growth of crystal nuclei into mature single crystals is poorly understood so far. A systematic variation of charge-balancing anions for a given metal/linker combination might thus serve the purpose of developing empirical framework design rules, particularly with respect to framework dimensionality, and thus path the way toward a rational (as opposed to a purely empirical) crystal engineering of novel framework compounds.[6,7] Cooperative covalent and non-covalent (*e.g.* templating effects through interactions such as hydrogen-bonding) interactions of anions can result in various topologies and framework dimensionalities within the same metal-linker system and thus help to select or energetically prefer a certain framework topology amongst different species.[6,8] Apart from this, other aspects, such as structure and functionality of the organic linker,[9,10] metal-linker ratio,[11] pH-value of the solution,[12,13] type of solvent or solvent mixture,[5,14] reaction temperature,[10,12,15,16] reaction time,[16,17] and templating effects[18] play a huge role for determining a final framework topology and dimensionality. In addition, thermal activation can open the door to establish a correlation between coordination frameworks of different dimensionality and topology, potentially transforming frameworks of low dimensionality (*i.e.*, one-dimensional, 1D, two-dimensional, 2D) into counterparts of higher dimensionality, and even provide access to potentially new or improved properties.[19] Here, we focus on the synthesis of various framework topologies of different dimensionality employing 1H,1′H-4,4′-bipyrazole (H_2BPZ) as organic linker in combination with Ni(II) and Co(II) salts, possessing different anions. Thirteen different structures have been obtained, with one being 1D, $Ni(H_2BPZ)(acac)_2$ (**1**); seven being 2D, $Ni(H_2BPZ)_2(H_2O)_2\cdot(NO_3)_2$ (**2**), $Ni_3(H_2BPZ)_6Cl_6\cdot(DMSO)_4$ (**3**), $Ni_8(H_2BPZ)_{16}Cl_{16}\cdot(DMSO)_6$ (**4**), $Ni(H_2BPZ)_2(H_2O)_6\cdot(ClO_3)_2(H_2O)_3$ (**5**), the isotypic structures $Ni(H_2BPZ)_2(CH_3SO_3)_2$ (**6**) and $Co(H_2BPZ)_2(CH_3SO_3)_2$ (**7**), and $Co(H_2BPZ)_2(CF_3SO_3)_2$ (**8**); and five being three-dimensional (3D), $Ni(H_2BPZ)_3\cdot(CF_3SO_3)_2$ (**9**), $Ni(H_2BPZ)_3\cdot(ClO_4)_2$ (**10**), $Co(H_2BPZ)_3\cdot(ClO_4)_2$ (**11**), $Ni(BPZ)\cdot(DMF)_{0.65}$ (**12**), and Ni(BPZ) (**13**). In the first 11 structures, the organic linker is incorporated into the framework in its neutral form with the anions counter-balancing the framework's charge, in the last two structures - in contrast - the linker is present in its deprotonated form, similar to a structure reported before.[20] Subsequent thermal activation allowed the transformation of 1D-, 2D-, and 3D-frameworks **1**, **3**, **6**, **9**, and **12** into 3D

[a] *R. Freund, M. Kraft, D. Volkmer*
Chair of Solid State and Materials Chemistry University of Augsburg
Institute of Physics
Universitaetsstrasse 1, 86159 Augsburg, Germany
E-mail: dirk.volkmer@physik.uni-augsburg.de

Supporting information for this article is available on the WWW under https://doi.org/10.1002/ejic.202100853

© 2021 The Authors. European Journal of Inorganic Chemistry published by Wiley-VCH GmbH. This is an open access article under the terms of the Creative Commons Attribution Non-Commercial NoDerivs License, which permits use and distribution in any medium, provided the original work is properly cited, the use is non-commercial and no modifications or adaptations are made.

© 2021 The Authors. European Journal of Inorganic Chemistry published by Wiley-VCH GmbH

Research Article
doi.org/10.1002/ejic.202100853

framework **13**, as well as 2D frameworks **7** and **8** into the 3D framework Co(BPZ)[20,21] (Scheme 1).

Results and Discussion

All obtained CPs have been characterized by light microscopy (Figure S1–S13), powder X-ray diffraction (PXRD, Figure S14–S25), thermogravimetric analysis (TGA) and variable temperature X-ray powder diffraction (VT-PXRD, S26–S47), IR spectroscopy (Figure S48–S60), UV/Vis spectroscopy (Figure S61–S71) and single crystal X-ray diffraction (see Table 1). In those cases where H_2BPZ is present in its doubly protonated forms, all cations are octahedrally coordinated, except of **12** and **13**, wherein nickel is placed in a square-planar coordination environment of deprotonated BPZ^{2-}.

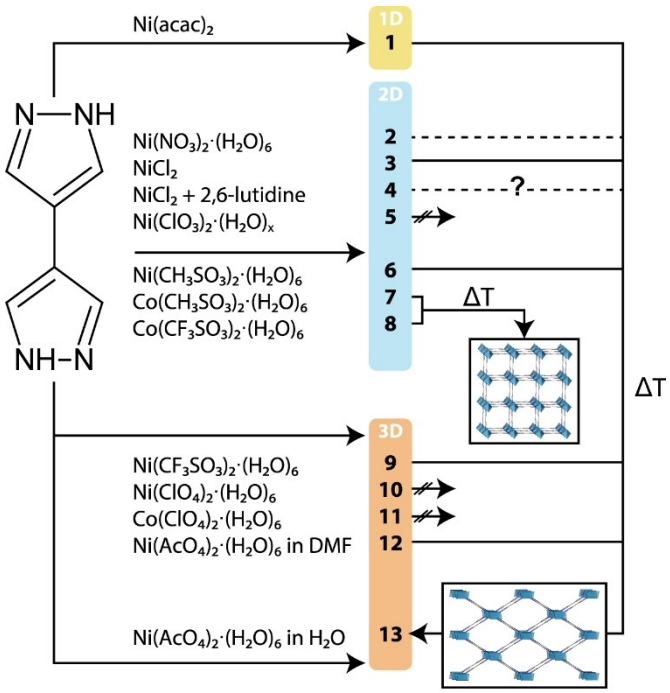

Scheme 1. Synthetic overview for structure **1** (1D), **2**–**8** (2D), and **9**–**13** (3D), where **1**, **3**, **6**, **9**, and **12** can be transformed into **13** and **7** and **8** into Co(BPZ) through elevated temperature.

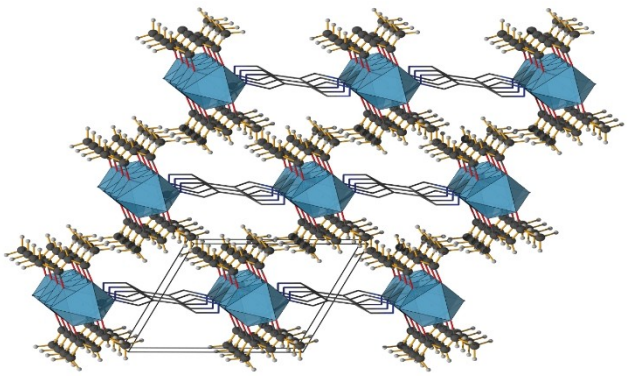

Figure 1. Crystal structure of $Ni(H_2BPZ)(acac)_2$ (**1**) constructed from 1D Ni-H_2BPZ chains.

One dimensional framework

The ethanolic reaction of $Ni(acac)_2$ with H_2BPZ resulted in large colorless triclinic single crystals of **1** crystallizing in the space group $P\bar{1}$ (no. 2). Each Ni^{2+} cation is octahedrally coordinated by four oxygen atoms originating from two bidentate acetylacetones in the equatorial plane and two nitrogen atoms of the axially bridging H_2BPZ molecules resulting in infinite, densely packed 1D chains running parallel to the *ac* plane (Figure 1). The Ni–O bond lengths in the octahedral NiN_2O_4 unit are 1.988 Å and 2.048 Å, respectively, and the N–N bond length is 2.140 Å, while the non-bonding distance between repeating Ni-unit is 10.098 Å. All atoms of the H_2BPZ linker are located in a common plane.

Two dimensional frameworks

Seven two-dimensional frameworks could be obtained deploying solvothermal reactions between various metal salts and H_2BPZ. $Ni(NO_3)_2\cdot(H_2O)_6$ and H_2BPZ in water yielded large light blue triclinic crystals of **2** crystallizing in the space group $P\bar{1}$ (no. 2), $NiCl_2$ and H_2BPZ in DMSO yielded light blue triclinic crystals of **3** crystallizing in the space group $P\bar{1}$ (no. 2) and light blue orthorhombic crystals of **4** crystallizing in the space group $C222_1$ (no. 20). $Ni(ClO_3)_2\cdot(H_2O)_x$ and H_2BPZ in ethanol and water yielded blue-violet orthorhombic crystals of **5** crystallizing in the space group $Cmc2_1$ (no. 36), $Ni(CH_3SO_3)_2\cdot(H_2O)_6$ and H_2BPZ and $Co(CH_3SO_3)_2\cdot(H_2O)_6$ and H_2BPZ in ethanol yielded the isotypic monoclinic 2D structures **6** and **7** in form of blue powder and big orange crystals, respectively, crystallizing in the space group $P2_1/n$ (no. 14). Finally, $Co(CF_3SO_3)_2\cdot(H_2O)_6$ and H_2BPZ in ethanol yielded big orange single crystals of **8** crystallizing in the space group $P\bar{1}$ (no. 2).

In all structures the metal cations are situated in octahedral coordination environment, with the equatorial plane being built up by four nitrogen atoms of coordinated H_2BPZ molecules. The axial positions of **2** and **5** are occupied by two oxygen atoms of coordinated neutral water molecules, while the axial positions of the other structures are coordinated by the respective anions.

For **2**, Ni–N bond lengths of 2.121 Å and 2.104 Å, respectively, and Ni–O bond length of 2.059 Å could be determined. As a result of this coordination environment, a 2D layer arrangement is formed with two displaced layers A and B with an A···A distance of 9.473 Å (Figure 2a). Similar to **1**, all atoms of the linker are placed in a common plane. Each NiN_4O_2-octahedron is surrounded by two non-coordinated NO_3^- anions forming discrete layers for counter-balancing the charges of the positively charged framework.

© 2021 The Authors. European Journal of Inorganic Chemistry published by Wiley-VCH GmbH

Table 1. Crystal data and structure refinement summary of $Ni(H_2BPZ)(acac)_2$ (**1**), $Ni(H_2BPZ)_2(H_2O)_2\cdot(NO_3)_2$ (**2**), $Ni_3(H_2BPZ)_6Cl_6\cdot(DMSO)_4$ (**3**), $Ni_8(H_2BPZ)_{16}Cl_{16}\cdot(DMSO)_6$ (**4**), $Ni(H_2BPZ)_2(H_2O)_6\cdot(ClO_3)_2(H_2O)_3$ (**5**), $Co(H_2BPZ)_2(CH_3SO_3)_2$ (**7**) (with $Ni(H_2BPZ)_2(CH_3SO_3)_2$ (**6**) being isotyp to **7**), $Co(H_2BPZ)_2(CF_3SO_3)_2$ (**8**), $Ni(H_2BPZ)_3\cdot(CF_3SO_3)_2$ (**9**), $Ni(H_2BPZ)_3\cdot(ClO_4)_2$ (**10**), $Co(H_2BPZ)_3\cdot(ClO_4)_2$ (**11**), $Ni(BPZ)\cdot(DMF)_{0.65}$ (**12**), and Ni(BPZ) (**13**). The data was collected using Mo-K_α radiation ($\lambda = 0.71703$ Å).

	1	**2**	**3**	**4**	**5**	**7**
Empirical formula	$C_{16}H_{20}N_4NiO_4$	$C_{12}H_{16}N_{10}NiO_8$	$C_{44}H_{60}Cl_6N_{24}Ni_3O_4S_4$	$C_{14}H_{18}Cl_2N_8NiOS$	$C_{14}H_{22}Cl_2N_8NiO_{11}$	$C_{14}H_{18}CoN_8O_6S_2$
M_r (g mol^{-1})	391.07	487.06	502.08	476.03	608.00	517.41
T (K)	300(2)	300(2)	297(2)	297(2)	83(2)	300(2)
Crystal dimensions (mm)	0.02×0.06×0.07	0.02×0.045×0.07	0.04×0.04×0.08	0.02×0.06×0.06	0.05×0.2×0.125	0.08×0.1×0.12
Crystal system	Triclinic	Triclinic	Triclinic	Orthorhombic	Orthorhombic	Monoclinic
Space group	P $\bar{1}$ (no. 2)	P $\bar{1}$ (no. 2)	P $\bar{1}$ (no. 2)	C 2 2 2_1 (no. 20)	C m c 2_1 (no. 36)	$P\,2_1/n$ (no. 14)
a (Å)	5.8072(2)	8.0632(3)	9.9762(4)	13.4860(5)	13.1548(17)	9.0820(2)
b (Å)	8.6070(3)	8.2638(3)	9.9778(4)	14.6967(5)	14.9233(14)	11.5312(2)
c (Å)	9.5513(4)	8.5731(3)	16.9575(5)	21.6497(8)	12.6598(13)	11.0021(2)
α (°)	65.0020(10)	106.8580(10)	87.0370(10)	90	90	90
β (°)	78.0430(10)	110.6580(10)	84.619(2)	90	90	107.7050(10)
γ (°)	84.8270(10)	104.1780(10)	86.4540(10)	90	90	90
V, (Å^3)	423.29(3)	471.52(3)	1675.51(11)	4291.0(3)	2485.3(5)	1097.64(4)
Z	1	1	3	8	4	2
D_c (g cm^{-3})	1.534	1.715	1.493	1.474	1.625	1.566
μ (mm^{-1})	1.175	1.097	1.256	1.271	1.065	1.020
F(000)	204	250	774	1952	1248	530
θ range (°)	2.39–30.00	2.79–27.50	2.29–26.50	2.26–26.50	2.06–26.50	2.56–30.00
Refl. collected	7218	16740	63472	40162	15251	31061
Refl. unique	7218	2165	6953	4451	2548	3201
Parameters/restraints	134/0	174/0	380/10	246/28	195/21	167/0
R(int)	0.0430	0.0397	0.0621	0.0474	0.0646	0.0495
GooF	1.045	1.045	1.039	1.087	1.072	1.095
R_1 [$I > 2\sigma(I)$][a]	0.0330	0.0266	0.0526	0.0445	0.0415	0.0368
wR_2 (all data)[b]	0.0770	0.0627	0.1288	0.1207	0.1006	0.0864
Largest diff. peak, hole (e Å^{-3})	0.635, −0.261	0.362, −0.241	0.781, −0.898	0.927, −0.896	0.418, −0.452	0.344, −0.735
	8	**9**	**10**	**11**	**12**	**13**
Empirical formula	$C_{14}H_{12}CoF_6N_8O_6S_2$	$C_{20}H_{18}F_6N_{12}NiO_6S_2$	$C_{18}H_{18}Cl_2N_{12}NiO_8$	$C_{18}H_{18}Cl_2CoN_{12}O_8$	$C_{7.97}H_4N_{4.66}NiO_{0.65}$	$C_6H_4N_4Ni$
M_r (g mol^{-1})	625.37	759.29	660.05	660.27	234.13	190.84
T (K)	297(2)	83(2)	299(2)	299(2)	303(2)	299(2)
Crystal dimensions (mm)	0.03×0.05×0.08	0.03×0.03×0.03	0.07×0.07×0.08	0.12×0.12×0.13	0.01×0.01×0.08	0.01×0.01×0.08
Crystal system	Triclinic	Trigonal	Trigonal	Trigonal	Orthorhombic	Orthorhombic
Space group	$P\,\bar{1}$ (no. 2)	$R\,\bar{3}$ (no. 148)	$R\,\bar{3}\,c$ (no. 167)	$R\,\bar{3}\,c$ (no. 167)	I m m a (no. 74)	I m m a (no. 74)
a (Å)	8.1485(4)	10.1157(3)	10.2330(3)	10.2538(4)	14.6077(5)	15.1089(8)
b (Å)	8.4068(4)	10.1157(3)	10.2330(3)	10.2538(4)	6.9426(2)	6.9090(4)
c (Å)	9.3081(5)	23.5617(11)	44.3309(13)	44.6785(16)	10.0037(4)	9.4550(6)
α (°)	89.748(2)	90	90	90	90	90
β (°)	68.462(2)	90	90	90	90	90
γ (°)	74.280(2)	120	120	120	90	90
V, Å^3	567.70(5)	2087.99(16)	4020.2(3)	4068.2(3)	1014.53(6)	986.98(10)
Z	1	3	6	6	4	4
D_c (g cm^{-3})	1.829	1.812	1.636	1.617	1.533	1.284
μ (mm^{-1})	1.040	0.950	0.991	0.897	1.883	1.913
F(000)	313	1152	2016	2010	471	384
θ range (°)	2.37–28.72	2.48–27.48	2.48–35.69	2.45–31.06	2.47–27.49	2.54–26.02
Refl. collected	25063	23585	35553	28483	10832	12640
Refl. unique	2939	1077	2074	1458	656	554
Parameters/restraints	169/0	72/0	88/0	88/0	50/1	29/0
R(int)	0.0760	0.0856	0.0352	0.0519	0.0555	0.1795
GooF	1.213	1.100	1.055	1.031	1.192	1.197
R_1 [$I > 2\sigma(I)$][a]	0.0808	0.0464	0.0405	0.0432	0.0345	0.0523
wR_2 (all data)[b]	0.1503	0.1078	0.1118	0.1078	0.0929	0.1076
Largest diff. peak, hole (e Å^{-3})	0.912, −0.593	0.646, −0.674	0.740, −0.506	0.588, −0.588	0.463, −0.590	1.408, −1.244

[a] $R_1 = \Sigma\,||F_o| - |F_c||/\Sigma|F_o|$. [b] $wR_2 = \Sigma[w(F_o^2 - F_c^2)2]/\Sigma[w(F_o^2)2]^{1/2}$.

In contrast, **3** and **4** form two differently stacked layered frameworks of similar composition. **3** possesses three displaced layers A, B, and C, with an A···A distance of 16.957 Å (Figure 2b). Within these layers, two different NiN_4Cl_2 coordination environments occur, one featuring Ni–N bond lengths of 2.090 Å and Ni–Cl bond lengths of 2.457 Å, respectively, the second featuring Ni–N bond lengths of 2.080 Å, 2.084 Å, 2.094 Å, and 2.100 Å and Ni–Cl bond lengths of 2.414 Å and 2.488 Å, respectively. The torsion angles between the pyrazole (pz) units in the linker molecules display different values, thus distorting the planar linkers. Depending on the linkers' positions in the framework, torsion angles of 160.61° and 168.26° occur within layer A and C, respectively, and a torsion angle of 180° in layer B (Figure 2b). On the other hand, **4** is constructed from four

© 2021 The Authors. European Journal of Inorganic Chemistry published by Wiley-VCH GmbH

Research Article
doi.org/10.1002/ejic.202100853

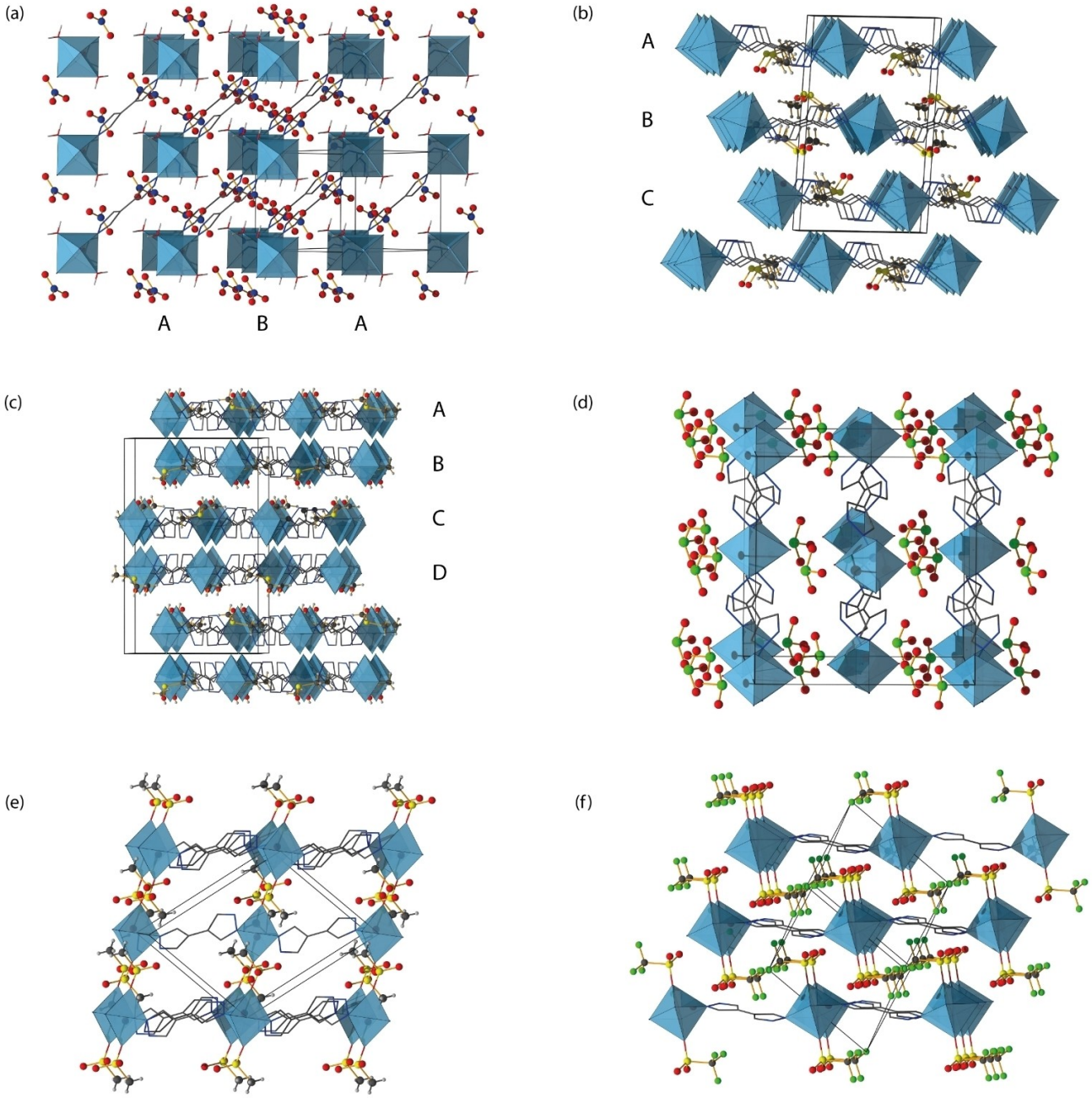

Figure 2. Crystal structures of (a) $Ni(H_2BPZ)_2(H_2O)_2 \cdot (NO_3)_2$ (**2**) a 2D framework with Ni-H_2BPZ-H_2O layers and uncoordinated NO_3^- anions for charge balance, (b) $Ni_3(H_2BPZ)_6Cl_6 \cdot (DMSO)_4$ (**3**) a 2D framework with three alternating layers, and (c) $Ni_8(H_2BPZ)_{16}Cl_{16} \cdot (DMSO)_6$ (**4**) a 2D framework with four alternating layers, (d) $Ni(H_2BPZ)_2(H_2O)_6 \cdot (ClO_3)_2(H_2O)_3$ (**5**) a 2D framework with Ni-H_2BPZ-H_2O layers and uncoordinated ClO_3^- anions in-between the layers, solvent not shown, (e) $Ni(H_2BPZ)_2(CH_3SO_3)_2$ (**6**) and $Co(H_2BPZ)_2(CH_3SO_3)_2$ (**7**) two 2D framework with coordinated methanesulfonate anions separating the layers, and (f) $Co(H_2BPZ)_2(CF_3SO_3)_2$ (**8**) a 2D framework with coordinated triflate anions separating the layers.

displaced layers A, B, C, and D with an A···A distance of 21.650 Å (Figure 2c). Here, the NiN_4Cl_2 coordination environment is identical for all Ni^{2+} cations, with Ni–N bond lengths of 2.079 Å, 2.080 Å, 2.091 Å, and 2.106 Å and Ni–Cl bond lengths of 2.418 Å and 2.489 Å, respectively. The torsion angles between the pz units in the linker molecules again are showing deviations from planarity, ranging from 161.88° to 157.74°. Both these structures contain solvent molecules occluded within the framework which can be removed by activation. While the reaction of **4** only resulted in a few single crystals suitable for single crystal X-ray analysis, **3** could be fully characterized (see section thermal analysis).

A coordination environment similar to **2** can be found for **5**. Here, the Ni–O bond lengths are 2.075 Å and 2.120 Å,

© 2021 The Authors. European Journal of Inorganic Chemistry published by Wiley-VCH GmbH

Research Article
doi.org/10.1002/ejic.202100853

respectively, and the Ni–N bond lengths 2.079 Å and 2.081 Å, respectively. The two off-set layers show an AB type succession with an A···A distance of 12.660 Å (Figure 2d). However, while in **2** the anions for the charge balance are found within the layer (Figure 2a), here the anions are exclusively in-between the layers. Besides, there is also further uncoordinated water and ethanol present within the structure (not visualized) which explains the increased distance in-between the layers compared to **2**. Differing from **2**, the torsion angle between the pz units in the linker molecules is 176.85°, deviating slightly from its energetically favorable planar conformation.

For **7** (and similarly for the isotypic structure **6**) the Co–O bond lengths of two $CH_3SO_3^-$ anions in the axial position counter-balancing the framework's charge are 2.098 Å and the Co–N bond lengths 2.115 Å and 2.121 Å, respectively. This arrangement dictates the layered composition of the structure, with $Co(H_2BPZ)^{2+}$-layers being separated by the anionic species with an interlayer distance of 8.302 Å (Figure 2e). Similar to **1** and **2**, the organic linker has a planar structure.

A very similar structural arrangement was obtained for **8**, where the Ni–O bond lengths for the triflate anions coordinated *via* an oxygen atom for charge balance are 2.118 Å and the Ni–N bond lengths 2.103 Å and 2.129 Å, respectively, the interlayer-distance 9.308 Å, and the torsion angle between the pz units in the linker molecules is 159.86°.

Three dimensional frameworks

In contrast to the 2D framework of **8**, the ethanolic reaction of $Ni(CF_3SO_3)_2\cdot(H_2O)_6$ with H_2BPZ resulted in the trigonal 3D framework of **9**, crystallizing in the space group $R\bar{3}$ (no. 148). Here, each Ni^{2+} cation is coordinated by six nitrogen atoms belonging to six H_2BPZ molecules with equal Ni–N bond lengths of 2.109 Å and surrounded by two $CF_3SO_3^-$ anions placed within the pores (Figure 3a). The pz units are not rotated relative to each other, which means a torsion angle of 180°. The isotypic structures **10** and **11**, both trigonal and crystallizing in the space group $R\bar{3}c$ (no. 167), are structurally very similar to **9**. However, the triflate anion is replaced by a perchlorate anion (Figure 3b). **10** is obtained from the solvothermal reaction of $Ni(ClO_4)_2\cdot(H_2O)_6$ and H_2BPZ in ethanol, **11** from the solvothermal reaction of $Co(ClO_4)_2\cdot(H_2O)_6$ and H_2BPZ in ethanol. The Ni center is octahedrally coordinated by six nitrogen anions of six H_2BPZ linker molecules with equal M–N bond lengths of 2.107 Å in **10** and 2.147 Å in **11**, respectively. Compared to all other structures discussed here, the torsion angle between the pz units of the bipyrazole linker reaches a maximum of 135.96° for **10**, and 134.87° for **11**, respectively. As illustrated in Figure 3a and b on the right, the charged entities of the frameworks **9**–**11** form pillars where one cation is invariably followed by two anions.

In contrast to all structures discussed before, where the protonated linker was incorporated within the framework, the structures **12** and **13** form a neutral framework of Ni^{2+} ions interconnected by bridging deprotonated BPZ^{2-} linkers (Figure 4), crystallizing in the space group *Imma* (no. 74). Deproto-

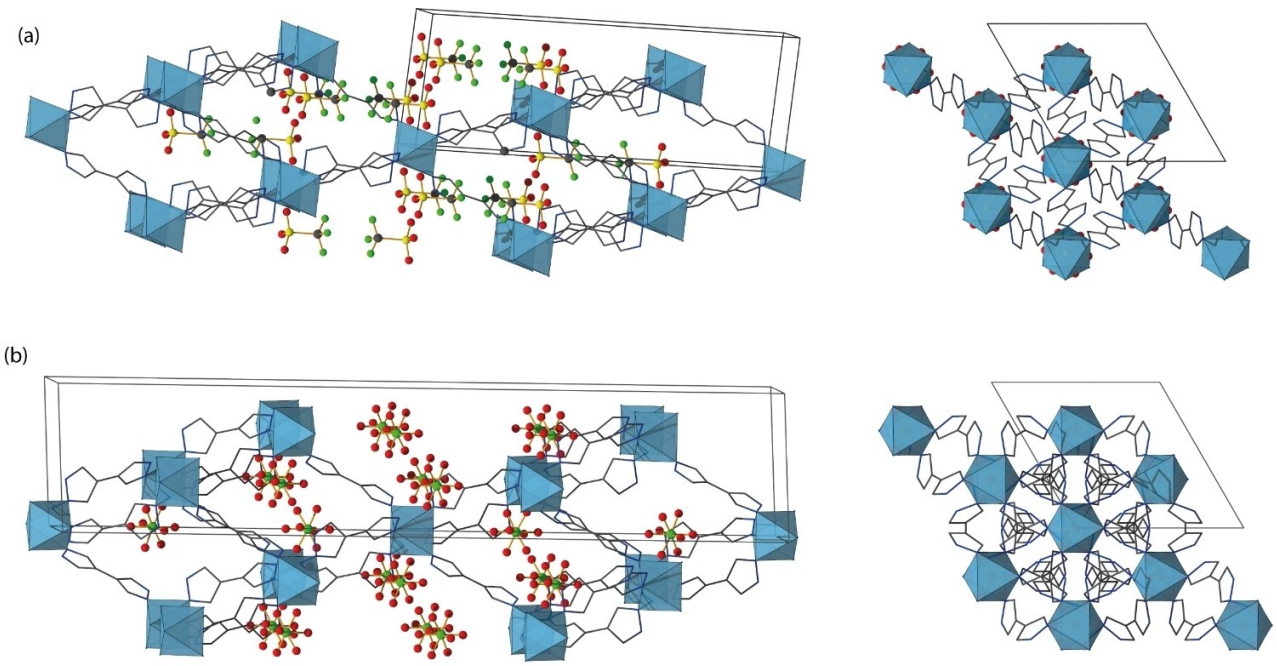

Figure 3. Crystal structure of (a) a 3D framework of $Ni(H_2BPZ)_2\cdot(CF_3SO_3)_2$ (**9**) with non-coordinated triflate anions counter-balancing the positive charges of the Ni-H_2BPZ framework, and (b) $Ni(H_2BPZ)_3\cdot(ClO_4)_2$ (**10**) and $Co(H_2BPZ)_3\cdot(ClO_4)_2$ (**11**), two 3D frameworks with non-coordinated perchlorate anions.

© 2021 The Authors. European Journal of Inorganic Chemistry published by Wiley-VCH GmbH

Research Article
doi.org/10.1002/ejic.202100853

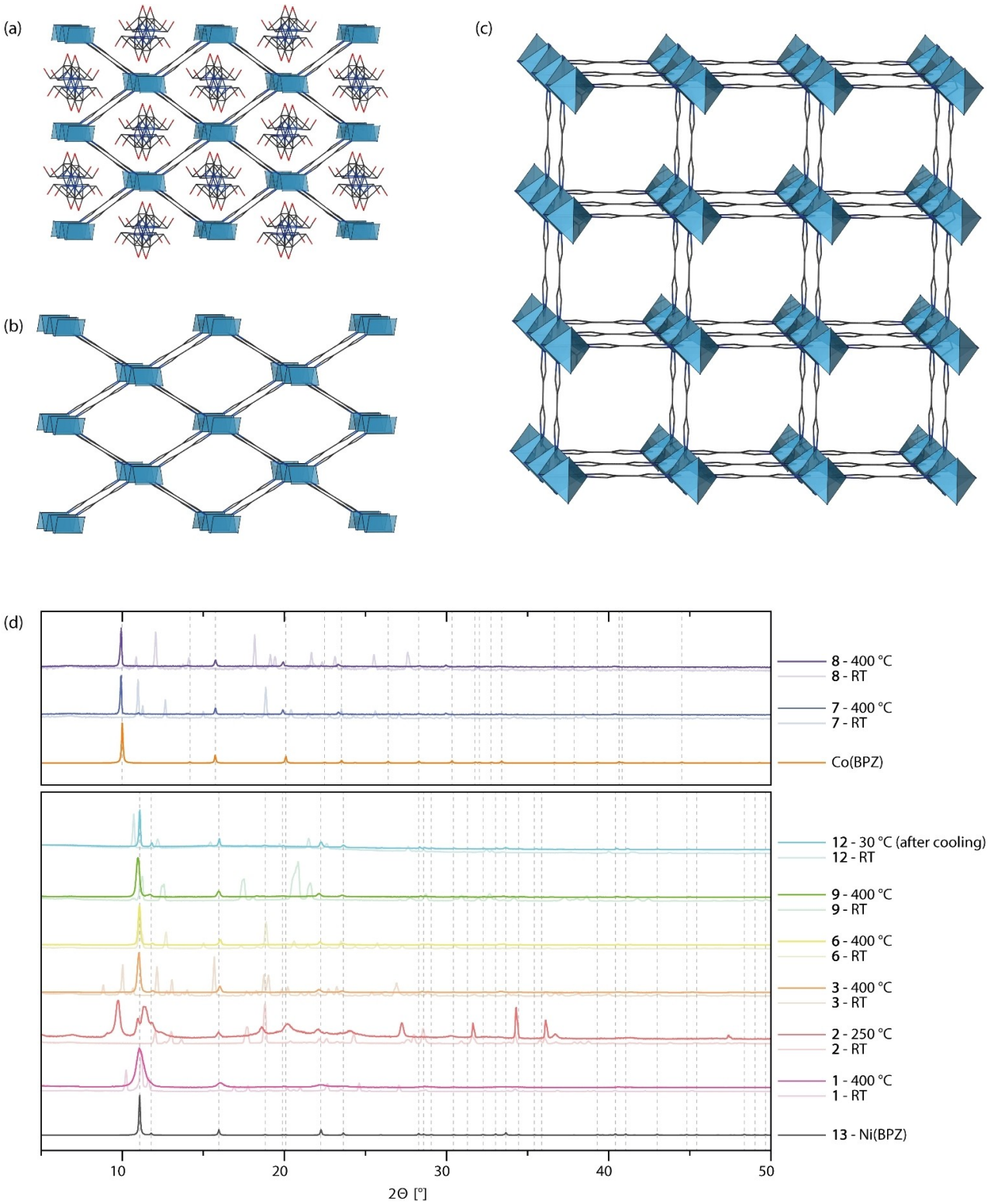

Figure 4. Crystal structure of (a) Ni(BPZ)·$(DMF)_{0.65}$ (**12**) a porous 3D network constructed from Ni^{2+} cations connected by bridging BPZ^{2-} linkers with disordered DMF within the pores, (b) Ni(BPZ) (**13**), a deformed analog of same topology, however, without coordinated solvent molecules within the pores, (c) Co(BPZ), the Co containing tetrahedral analog of Ni(BPZ), and (d) an overview of the results of the transformations of the corresponding structures into the 3D structure **13** as well as Co(BPZ) based on the high-temperature PXRD measurements obtained via VT-PXRD.

nation of the linker is accompanied by a change in the coordination environment, with nickel now being square planar coordinated, with much shorter Ni–N bond lengths of 1.889 Å for **12** and 1.906 Å for **13**, respectively. The torsion angle

© 2021 The Authors. European Journal of Inorganic Chemistry published by Wiley-VCH GmbH

Research Article
doi.org/10.1002/ejic.202100853

between the pyrazolate units in the deprotonated linker is 180° in both structures. While **12** is present with DMF within the pores, **13** forms as a neutral framework free of strongly adsorbed solvent. This lack of interaction explains both the differences in lattice parameters observed here and the associated high structural dependence on the solvent reported before.[20,22]

Thermal analysis

TGA was performed to obtain information on possible 1D-3D, 2D-3D, and 3D-3D phase transitions by means of the mass changes as a function of temperature and to investigate the thermal stability of the different structures obtained. Phase transitions are expected owing to the incorporation of electrostatically neutral linker molecules into the framework. Removal of volatile components, such as the fully protonated forms of the charge-balancing anions, upon heating could establish new linker connections, after transfer of the protons onto the anions. And as expected, corresponding transformations could be observed for networks of every dimension. The 1D network **1**, as well as the 2D networks **2**, **3** (presumably as a transition state), **6**, **7**, and **8**, and the 3D network **9** could be transformed into corresponding 3D networks (Figure 4d).

The TGA of **1** revealed 3 steps of mass loss (Figure S26). Using the results of the VT-PXRD analysis (Figure S27), the first step of mass loss (35.5% between 180 and 280 °C) can be attributed to the formation of the pyrazolate with the release of acetylactone triggering a 1D-3D transformation of framework **1** into **13** (Figure 4b and d), while the subsequent two steps of mass loss can be assigned to the degradation of linker and framework. The calculated mass loss for the first step is about 52%, which implies that the release of acetylacetone is incomplete. The coordination environment of the Ni^{2+} cation changes during the phase transition from octahedral (*2 C1* topology[23]) to square-planar (*sqc176* topology[23]) with two BPZ^{2-} molecules bridging the metal centers, forming infinite 3D interconnected Ni-BPZ-chains throughout the framework. This change in coordination environment goes hand in hand with a change in color from colorless to orange. This *via* phase transition obtained crystal phase is stable up to around 475 °C.

TGA of 2 (Figure S28) shows several steps of mass loss. The first mass loss between 90 and 140 °C equals 7.6% and can be attributed to the release of water (calculated 7.4%), with the nitrate anions presumably occupying the axial sites in the coordination environment of the nickel cation replacing the water molecules. Between 200 and 470 °C another four steps of mass loss can be observed. The first mass loss between 200 and 300 °C can potentially be attributed to the partial release of HNO_3 (21.3% measured compared to 25.5% calculated) which in turn would indicate the deprotonation of the organic linker and the formation of new bonds. While some correspondence of reflex positions is observed upon comparison of the PXRD data, which may indicate the formation of bonds analogous to **13** (for 250 °C in the VT-PXRD, Figure S29 and Figure 4b and Figure 4d), the full transition towards a framework analogous to **13** as a pure phase cannot be observed at any temperature. Accordingly, new linkages analogous to **13** are formed at best as a transition state towards the decomposition to nickel oxide at about 300 °C.

Similarly, structure **3** displays a hand full steps of mass loss during TGA (Figure S30). The first mass loss between 70 and 150 °C can be attributed to the release of ethanol, stemming from the washing procedure (see experimental section) followed by the release of hydrochloric acid between 150 and 280 °C resulting from the deprotonation of the organic linker and the concomitant release of protonated chloride (HCl) (14.7% measured compared to 14.5% calculated). In this process, at around 338 °C, the structure undergoes a 2D-3D phase transition resulting in the formation of **13** (Figure 4b and Figure 4d), as identified through VT-PXRD (Figure S31), while releasing 3 molecules of linker per formula unit (see eq. 1 in the SI). At the same time DMSO is released, but residual quantities of the solvent remain in the framework, since the measured mass loss of 32.2% does not correspond to the 47.5% calculated for complete release. The obtained phase, indicated through a change of color from light blue to orange, is stable up to around 550 °C where it spontaneously decomposes under the formation of nickel oxide.

Thermal analysis of **4** was due to the extremely low yields not possible. On the other hand, **5** showed thermal behavior completely different from the other compounds. In TGA (Figure S32), two ranges can be distinguished, on the one hand a mass loss of approx. 17% up to a temperature of approx. 100 °C which can be assigned to evaporation of solvent, on the other hand a spontaneous mass loss of nearly 80% at 201 °C. What can be observed here is the spontaneous decomposition of the chlorate anion incorporated in the structure; this explosive nature could also be illustrated by simple heating experiments in the fume hood.

As expected, the isotypic compounds **6** and **7** both behave very similarly in the thermal analysis (Figure S34 - S37). Both structures are thermally stable up to a temperature of about 350 °C, after which a 2D-3D phase transition occurs (see eq. 3 and 4 in the SI) that is completed at about 400 °C (with observed mass losses of approx. 58% for both structures, calculated: 63%). Further steps of mass loss can be attributed to the evaporation of excess linker molecules remaining from the phase transition and subsequent decomposition of the 3D framework at temperatures of 500 °C and above. Even though the mechanism of the 2D-3D phase transitions can be considered similar due to the similar thermal behavior, the product for **6** and **7** is different. While the nickel structure **6** leads to the formation of the 3D structure **13** (Figure 4b and d), the cobalt structure **7** forms the 3D framework Co(BPZ)[20,21] which crystallizes in the tetragonal space group $P4_2/mmc$ (no. 131, Figure 4c and d). Cobalt is tetrahedrally surrounded by 4 nitrogen atoms of 4 linker units (*sqc183* topology[23]), which leads to the formation of infinitely long Co chains, where each cation is bridged by 90° altering linkers.

The thermal behavior of **8** is very similar to that of **7**, with the phase transition only occurring at somewhat higher temperatures (Figure S38 and 39, Figure 4d). Here, too, a mass loss of

© 2021 The Authors. European Journal of Inorganic Chemistry published by Wiley-VCH GmbH

just some 60% can be observed, compared to a calculated value of approx. 69%. Accordingly, some organic linker molecules remain in the newly formed 3D framework during the phase transformation, which only evaporate at higher temperatures in the course of framework decomposition from about 500 °C onward. In contrast to **7**, however, an increasing amorphization of the framework can already be observed at 425 °C for **8**, with more and more decreasing intensities in the measured PXRD patterns.

A 3D-3D phase transition could be observed for **9** at elevated temperatures. Conversely, while TGA has only shown a mass loss of 17.2% within a temperature range of 260 up to 400 °C (Figure S40), one would expect a mass loss of 74.6% for a similar phase transformation. Accordingly, the majority of the substances released from the heated framework must remain within the structure, being released only upon complete decomposition at about 500 °C under formation of nickel oxide. However, the fact that such a 3D-3D phase transformation occurs at all can be derived from the VT-PXRD measurement (Figure S41, Figure 4d), where at a temperature above 400 °C only **13** (Figure 4b) can be recognized as crystalline phase.

The results of the thermal investigations for **10** and **11** are similar, with both compounds showing thermal stability up to approx. 400 °C, the nickel compound showing somewhat higher stability (Figure S42–45). Up to these temperatures, only slight, thermally induced distortions of the framework occur, above which decomposition occurs with the formation of the corresponding metal oxides.

Lastly, **12** was examined thermally (Figure S46 and 47), and as the temperature increases and the solvent evaporates, a deformation of the framework towards **13** (Figure 4a, Figure 4b, and Figure 4d) can be observed due to the removal of DMF from the framework (as indicated by FT-IR spectroscopy, Figure S60) and the interactions associated with it. Similar solvent-dependent structural relationships for Ni(BPZ) frameworks have already been observed and described in literature.[20,22] In addition, **13** can also be obtained via direct synthesis from aqueous reaction mixtures.

In summary, the following observation can be made with respect to thermal analysis. Even if a large number of low-dimensional frameworks are available as a starting point, almost all of them could be transformed into 3D frameworks by thermal activation (Scheme 1, Figure 4d). Both 1D and 2D frameworks could be successfully transformed, except for **5**, which spontaneously decomposed already at lower temperatures due to the explosive nature of the chlorate anion. Even though a thermal analysis of **4** was not possible due to low yields, it can be assumed that a 2D-3D phase transition should also be likely here due to the high structural similarity with **3**. A 3D-3D phase transition was also observed for **9**, in contrast to compounds **10** and **11**, which only decomposed upon thermal activation. The 3D structure **12**, in which the organic linker was already deprotonated, could be transferred analogously to the low-dimensional nickel frameworks in **13**, whereby here only structural distortions occur owing to the removal of the solvent. The cobalt structures **7** and **8** form Co(BPZ) during thermal activation, the tetragonal analog of the Ni(BPZ).

UV/Vis spectroscopy

The spectra of the UV/Vis spectroscopic analysis can be found in the SI as Figure S61–S71.

d^8-Ni(II) has 3 spin-allowed transitions, namely the transitions from $^3A_{2g}\rightarrow{}^3T_{2g}$, $^3A_{2g}\rightarrow{}^3T_{1g}(F)$, and $^3A_{2g}\rightarrow{}^3T_{1g}(P)$. A summary of the band maxima, assignments, and calculated values for B and Δ_O can be found in Table S1 of the SI. The energies of the bands appearing in the spectra are in good agreement with values already known from the literature. The different transitions $^3A_{2g}\rightarrow{}^3T_{2g}$, $^3A_{2g}\rightarrow{}^3T_{1g}(F)$, and $^3A_{2g}\rightarrow{}^3T_{1g}(P)$ can be observed for **1** at 23,000, 16,900, and 10,000 cm^{-1}, for **2** at 27,600, 16,000, and 10,500 cm^{-1},[24] for **3** at 26,100, 16,500, and 10,500 cm^{-1},[25] for **5** at 29,300, 17,000, and 10,500 cm^{-1}, for **6** at 27,000, 17,000, and 10,400 cm^{-1}, for **9** at 27,900, 17,300, and 10,500 cm^{-1}, and for **10** at 28,200, 17,700, and 10,800 cm^{-1}.[25,26] The Racah parameter B and the crystal field splitting parameter Δ_O are thereby calculated to be 557 and 10,028 cm^{-1} for **1**, 832 and 10,646 cm^{-1} for **2**, 760 and 10,569 cm^{-1} for **3**, 1037 and 10,677 cm^{-1} for **5**, 837 and 10,714 cm^{-1} for **6**, 934 and 10,831 cm^{-1} for **9**, and 873 and 10828 cm^{-1} for **10**.

d^7-Co(II) has 3 spin-allowed transitions, the transitions from $^4T_{1g}(F)\rightarrow{}^4T_{2g}$, $^4T_{1g}(F)\rightarrow{}^4T_{1g}(P)$, and $^4T_{1g}(F)\rightarrow{}^4A_{2g}$, with the results again summarized in Table S1 of the SI. The energies of the bands appearing in the spectra agree with values known from the literature and can be assigned as follows. $^4T_{1g}(F)\rightarrow{}^4T_{2g}$, $^4T_{1g}(F)\rightarrow{}^4T_{1g}(P)$, $^4T_{1g}(F)\rightarrow{}^4A_{2g}$, B, and Δ_O can be determined, or calculated, respectively to 20,900, 19,300, 10,000, 678, and 11181 cm^{-1} for **7**, to 20,800, 19,000, 10,000, 673, and 11112 cm^{-1} for **8**, and to 21,600, 20,200, 10,000, 780, and 11234 cm^{-1} for **11**.[26,27]

Comparing the crystal field splitting from the Ni^{2+} to Co^{2+} compounds, we find larger values for the splitting of the cobalt compounds as one would expect, considering their positions in the spectrochemical series of metal ions.[28] Comparing the nickel compounds with each other, the calculated ligand field splittings coincide well with what one could expect with respect to the spectrochemical series of the ligands.[29] Pz can be ranked in the spectrochemical series as a ligand with a somewhat stronger ligand-field splitting, roughly on the order of other unidentate nitrogen donors such as ammonia or methylamine.[24,25] Thus, one would expect the following increase in ligand-field splitting: $Cl^- < H_2O <$ $acac^- < CH_3SO_3^- \sim CF_3SO_3^- <$ pyrazoles. Since both $CH_3SO_3^-$ and $CF_3SO_3^-$ coordinate via oxygen, the splitting of the two should not differ greatly, which is indeed the case. **1** shows the weakest splitting due to the fact that only 2 pz moieties and 2 $acac^-$ anions make up the nickel environment, followed by **3** (4 pz, 2 Cl^-), **2** and **5** (4 pz, 2 H_2O), **6** (4 pz, 2 CH_3SO_3), and **9** and **10** (6 pz). The same trend can be seen for the cobalt complexes, with **7** (4 pz, 2 CH_3SO_3) and **8** (4 pz, 2 CF_3SO_3) showing similar splitting values, and **11** (6 pz) showing a larger one.

Role of the anion for crystal structure and size. After the full characterization of the obtained structures, the next step was to investigate the role of the anions in relation to the framework dimensionality and crystal morphology of the obtained structures, with emphasis on the coordination

© 2021 The Authors. European Journal of Inorganic Chemistry published by Wiley-VCH GmbH

Research Article
doi.org/10.1002/ejic.202100853

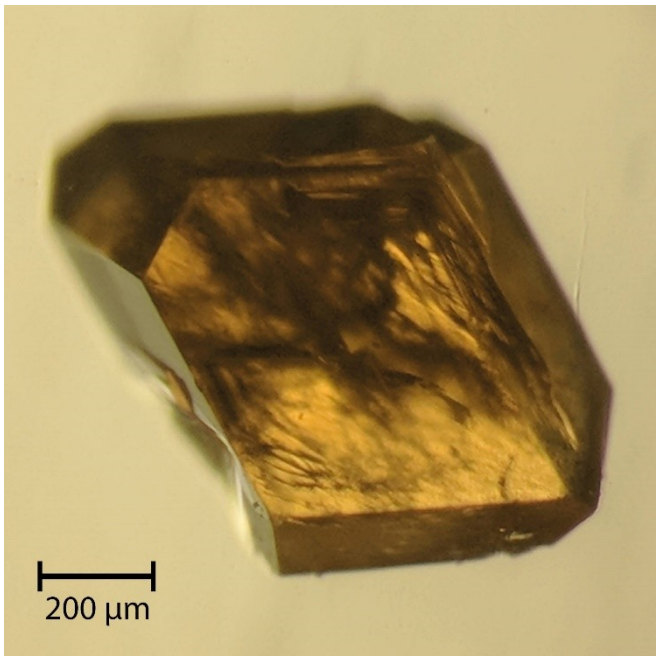

Figure 5. Image of **11** obtained with a camera through a microscope displaying its remarkable size.

strength of the anions. If the organic linker is deprotonated, frameworks can be formed without the inclusion of anions, since the organic linker alone can be sufficient to balance the charge. However, since in this case linker and anion are one and the same and the coordination strength towards the metal center is much larger compared to the case of neutrally coordinated linkers, the solubility of the product decreases, which in turn results in the crystals of these structures usually not growing as large.

In structures where the linker is neutrally incorporated into the framework, anions are present for charge balancing, which, alongside the reaction aspects addressed in the introduction, have a key role to play with respect to crystal structure and size. Through characteristics such as coordination strength, structure and size of the anion, charge distribution, templating effects, and denticity, they exert a subtle influence on the dimensionality of the framework depending on the coordination number and type (*e.g.*, anions can also bridge metal centers) and ultimately also have a significant influence on the crystal size, which is also influenced by the solubility of the metal salts as a function of the coordination strength of the anions themselves. This coordination strength is one of the most important properties of the anion, with the organic linker competing with the anion for the metal center. If the linker is deprotonated, the coordination strength is considerably stronger, and the anion is usually displaced from the metal's coordination sphere. In the neutral state, however, the coordination strength of the linker is substantially weakened, and the coordination strength of the anion take over a dominant role.

The anions used in this study can be ranked in terms of their coordination strength as follows: $acac^- > Cl^- > CH_3SO_3^- > ClO_3^- > NO_3^- > CF_3SO_3^- > ClO_4^-$.[29,30] This trend can also be confirmed on the basis of the coordination environments of the obtained structures, where **1** is 1D due to the chelating effect of the $acac^-$ anion, **28** are 2D owing to the strong to moderate coordination strength (with exception of **3** and **5**, where water occupies the axial coordination positions), and **9**–**11** are 3D because of the weak coordination strength of the anion. While this trend is not reflected as markedly in crystal size, a rough pattern can be discerned, with **12** and **13** being microcrystalline and **1**–**11** taking dimensions of up to several 100 µm. In particular, **11** stands out, with maximum crystal dimensions of over 1 mm (Figure 5).

Conclusion

Here we reported a total of thirteen structures of different dimensionalities built from Ni^{2+} or Co^{2+} metal centers and 1H,1′H-4,4′-bipyrazole as organic linker. Eleven structures incorporated the linker into the framework in neutral form, which necessitated the presence of anions to counterbalance the electrostatic charge within the framework, influencing structure, dimensionality, and crystal size. Two frameworks bound the linker in deprotonated form, eliminating the need for anions to balance the charge.

Furthermore, the structures were investigated for their thermal behavior. It was observed that by thermal activation, it was possible to transfer protons from the linker to the anions, with the newly formed volatile molecular species evaporating, resulting in the formation of the Ni(BPZ) framework **13** or the tetragonal analog Co(BPZ) framework for most of the reported structures. This phase transition could be observed both for 1D, 2D, and 3D structures.

Overall, we were able to show the structural diversity of the Ni/Co-H_2BPZ system, the supporting role of anions in it, the diversity in low-dimensional to 3D phase transformations, and the resulting underlying influence on framework dimensionality.

Experimental Section

Chemicals and Materials. 1H,1′H-4,4-bipyrazole (H_2BPZ)[31] and hexakis(μ^2-3-phenylpyrazolato)trinickel(II)[32] were prepared using previously reported methods. $Ni(SiF_6)\cdot(H_2O)_6$ was obtained through the reaction of Ni (1.0 g, 17.0 mmol) with hexafluorosilicic acid (6.4 mL, 20.0 mmol) in 5 mL water stirred at 100 °C for 20 h. After hot filtration the pure product was obtained by precipitation with acetone (4.96 g, yield: 95 %). $Ni(ClO_3)_2\cdot(H_2O)_x$ was obtained through a salt metathesis reaction of $Ni(SiF_6)\cdot(H_2O)_6$ (617.5 mg, 2.0 mmol) and $KClO_3$ (490.6 mg, 4.0 mmol) dissolved in 50 mL of water. The mixture was stirred for 1 h at room temperature and then dried at 60 °C overnight for the water to evaporate. The pure lime green product can be obtained by dissolution in 15 mL MeOH, filtration for the removal of undissolved K_2SiF_6, and subsequent solvent removal at 100 °C under vacuum (340.2 mg, yield: 75 %). $Ni(CH_3SO_3)_2\cdot(H_2O)_6$ was obtained through the reaction of Ni (1.0 g, 17.0 mmol) with methanesulfonic acid (2.2 mL, 34.0 mmol) in 5 mL water stirred at 100 °C for 3.5 h. After hot filtration the water was left to evaporate overnight at room temperature and the pure

© 2021 The Authors. European Journal of Inorganic Chemistry published by Wiley-VCH GmbH

green product was obtained by re-dispending the solid in THF followed by filtration (5.84 g, yield: 97%). $Co(CH_3SO_3)_2 \cdot (H_2O)_6$ was obtained through the reaction of Co (1.0 g, 17.0 mmol) with methanesulfonic acid (2.2 mL, 34.0 mmol) in 5 mL water stirred at 100 °C for 3.5 h. After hot filtration the water was left to evaporate overnight at room temperature and the pink liquid was mixed with THF for the removal of remaining water and acid and subsequently isolated. For crystallization of the pure product the liquid was placed in ice and then dried overnight at 100 °C under vacuum (4.82 g, yield: 80%). $Ni(CF_3SO_3)_2$ was obtained through the reaction of Ni (5.0 g, 85.2 mmol) with triflic acid (15.0 mL, 170.0 mmol) in 25 mL water stirred at room temperature overnight. The solution was then heated to 100 °C, the solvent removed using a rotary evaporator, and then dried at 100 °C under vacuum overnight to obtain the pure yellow product (29.87 g, yield: 98%). $Co(CF_3SO_3)_2$ was obtained through the reaction of Co (1.0 g, 17.0 mmol) with triflic acid (3.0 mL, 34.0 mmol) in 5 mL water stirred at 100 °C for 2 h. The mixture was then filtrated and dried at 100 °C under vacuum overnight to obtain the pure pink product (5.78 g, yield: 96%). All the other chemicals are commercially available. The solvents used were of analytical grade and were used without further purification.

Characterization. Fourier transform infrared (FT-IR) spectroscopy was carried out using a Bruker Equinox 55 FT-IR spectrometer with an ATR unit in the range 4000 to 400 cm^{-1}. TGA was performed with a TA Instruments Q500 device in the temperature range of 25 °C–700 °C under flowing nitrogen at a heating rate of 10 $Kmin^{-1}$. Diffuse reflectance UV-vis-NIR spectra were recorded in the range of 1500–200 nm on a PerkinElmer λ750s spectrometer equipped with a Labsphere 60 mm RSA ASSY integrating sphere with a 0°/d measuring geometry. Labsphere Spectralon SRS-99 was used as the white standard. X-ray powder diffraction (PXRD) data were collected in the 4–40° 2θ range using a Seifert XRD 3003 TT-powder diffractometer with a Meteor1D detector operating at room temperature using Cu $K\alpha_1$ radiation (λ = 1.54187). Variable temperature powder X-ray diffraction (VT-PXRD) measurements were collected in the 2θ range of 5–70° with 0.02° steps with an Empyrean (PANalytical) Diffractometer equipped with a Bragg-BrentanoHD mirror, a PIXcel3D 2×2 detector and a XRK 900 reactor chamber (Anton Paar). Single crystal X-ray diffraction measurements were conducted by mounting a single crystal on a MiTeGen MicroMount and collecting the X-ray reflection data set using a Bruker D8 Venture diffractometer. Intensity measurements were carried out using monochromatic (doubly curved silicon crystal) Mo Kα radiation (0.71073 Å) emitted from a sealed microfocus tube with generator setting of 50 kV and 1 mA. Integrated intensities and unit cell refinements were performed using the Bruker SAINT software package. The structures were solved by direct methods and refined using the SHELXL 2018/3 program.[33]

Synthesis of $Ni(H_2BPZ)(acac)_2$ (1): $Ni(acac)_2$ (26.7 mg, 0.10 mmol) was dissolved in 2 mL of ethanol and mixed with H_2BPZ (6.6 mg, 0.05 mmol) in a glass tube which was closed with a plastic cap and then heated to 90 °C under solvothermal conditions for 3 days. The resulting light blue crystals were filtered off and washed with ethanol. IR bands (cm^{-1}): 3275 (br), 3075 (w), 3001 (w), 2964 (w), 1584 (m), 1509 (s), 1470 (m), 1402 (s), 1364 (m), 1300 (m), 1260 (m), 1216 (m), 1192 (w), 1165 (w), 1152 (w), 1117 (s), 1063 (m), 1037 (m), 1013 (m), 962 (m), 922 (m), 911 (m), 849 (m), 814 (m), 766 (m), 741 (m), 656 (m), 614 (m), 579 (m), 464 (w), 424 (m). Yield: 62%.

Synthesis of $Ni(H_2BPZ)_2(H_2O)_2 \cdot (NO_3)_2$ (2): $Ni(NO_3)_2 \cdot (H_2O)_6$ (29.4 mg, 0.10 mmol) was dissolved in 2 mL of water and mixed with H_2BPZ (6.7 mg, 0.05 mmol) in a glass tube which was closed with a plastic cap and then heated to 90 °C under solvothermal conditions for 3 days. The resulting light blue crystals were filtered off and washed with ethanol. IR bands (cm^{-1}): 3356 (w), 3256 (br), 3138 (w), 2975 (w), 1669 (w), 1536 (w), 1484 (m), 1464 (s), 1381 (s), 1341 (s), 1301 (m), 1242 (m), 1156 (w), 1129 (s), 1042 (s), 955 (m), 908 (m), 867 (s), 821 (m), 775 (m), 726 (m), 710 (w), 681 (m), 648 (m), 595 (s). Yield: 56%.

Synthesis of $Ni_3(H_2BPZ)_6Cl_6 \cdot (DMSO)_4$ (3): $NiCl_2$ (6.4 mg, 0.05 mmol) was dissolved in 2 mL of DMSO and mixed with H_2BPZ (26.7 mg, 0.20 mmol) dissolved in 2 mL of DMSO in a glass tube which was closed with a plastic cap and then heated to 110 °C under solvothermal conditions for 3 days. The resulting light blue crystals were filtered off and washed with DMSO and ethanol. IR bands (cm^{-1}): 3257 (br), 3113 (w), 1631 (w), 1524 (w), 1483 (w), 1458 (w), 1377 (m), 1311 (w), 1227 (w), 1159 (m), 1127 (m), 1040 (s), 959 (m), 910 (s), 865 (m), 817 (m), 764 (m), 695 (m), 669 (w), 651 (w), 608 (m), 592 (m). Yield: 61%.

Synthesis of $Ni_8(H_2BPZ)_{16}Cl_{16} \cdot (DMSO)_6$ (4): $NiCl_2$ (12.7 mg, 0.10 mmol) was dissolved in 2 mL of DMSO and mixed with H_2BPZ (12.5 mg, 0.09 mmol) dissolved in 2 mL of DMSO in a glass tube which was after addition of 125 μL of 2,6-lutidine closed with a plastic cap and then heated to 110 °C under solvothermal conditions for 2 days. The few resulting light blue crystals were directly picked for single crystal analysis.

Synthesis of $Ni(H_2BPZ)_2(H_2O)_6 \cdot (ClO_3)_2(H_2O)_3$ (5): $Ni(ClO_3)_2 \cdot (H_2O)_x$ (30.0 mg, 0.09 mmol) was dissolved in 1 mL of ethanol and 0.25 mL of water and mixed with H_2BPZ (13.4 mg, 0.05 mmol) in a glass tube which was closed with a plastic cap and then heated to 45 °C under solvothermal conditions for 12 days. The resulting blue-violet crystals were filtered off and washed with ethanol. IR bands (cm^{-1}): 3241 (br), 3132 (w), 2973 (w), 1640 (w), 1544 (w), 1474 (w), 1392 (m), 1347 (w), 1318 (w), 1255 (w), 1163 (w), 1137 (s), 1049 (s), 989 (w), 940 (s), 908 (s), 875 (w), 841 (w), 740 (w), 601 (m), 470 (m), 455 (w). Yield: 35%.

Synthesis of $Ni(H_2BPZ)_2(CH_3SO_3)_2$ (6): $Ni(CH_3SO_3)_2 \cdot (H_2O)_6$ (14.4 mg, 0.04 mmol) was dissolved in 4 mL of ethanol and mixed with H_2BPZ (13.4 mg, 0.10 mmol) in a glass tube which was closed with a plastic cap and then heated to 65 °C under solvothermal conditions for 2 days. The resulting light blue powder was filtered off and washed with ethanol. IR bands (cm^{-1}): 3273 (br), 3128 (br), 3048 (w), 2979 (w), 1546 (w), 1518 (w), 1480 (w), 1414 (w), 1390 (w), 1334 (w), 1319 (w), 1228 (s), 1174 (s), 1162 (s), 1121 (s), 1048 (s), 967 (m), 957 (m), 914 (m), 894 (m), 853 (m), 790 (m), 773 (s), 736 (m), 672 (m), 656 (m), 614 (m), 552 (s), 541 (s), 522 (s), 467 (m), 426 (m). Yield: 71%.

Synthesis of $Co(H_2BPZ)_2(CH_3SO_3)_2$ (7): $Co(CH_3SO_3)_2 \cdot (H_2O)_6$ (14.3 mg, 0.04 mmol) was dissolved in 4 mL of ethanol and mixed with H_2BPZ (13.2 mg, 0.10 mmol) in a glass tube which was closed with a plastic cap and then heated to 90 °C under solvothermal conditions for 3 days. The resulting orange crystals were filtered off and washed with ethanol. IR bands (cm^{-1}): 3169.93 br), 2979.94 (w), 1483 (w), 1416 (w), 1388 (w), 1335 (w), 1319 (w), 1228 (m), 1162 (m), 1122 (m), 1047 (s), 966 (m), 957 (m), 914 (m), 893 (m), 856 (m), 774 (m), 745 (m), 673 (m), 656 (m), 615 (m), 553 (s), 541 (s), 526 (s), 425 (m). Yield: 63%.

Synthesis of $Co(H_2BPZ)_2(CF_3SO_3)_2$ (8): $Co(CF_3SO_3)_2 \cdot (H_2O)_6$ (18.5 mg, 0.05 mmol) was dissolved in 2 mL of ethanol and mixed with H_2BPZ (7.2 mg, 0.05 mmol) in a glass tube which was closed with a plastic cap and then heated to 70 °C under solvothermal conditions for 4 days. The resulting orange crystals were filtered off and washed with ethanol. IR bands (cm^{-1}): 3372 (w), 3240 (br), 3109 (w), 3051 (w), 2864 (w), 1649 (w), 1538 (w), 1469 (w), 1393 (w), 1376 (w), 1296 (s), 1257 1226 (s), 1180 (m), 1161 (m), 1132 (s), 1040 (s), 964 (m), 909 (m), 866 (s), 829 (m), 813 (m), 763 (w), 693 (m), 651 (m), 634 (m), 614 (m), 593 (m), 580 (m), 516 (s). Yield: 49%.

© 2021 The Authors. European Journal of Inorganic Chemistry published by Wiley-VCH GmbH

Synthesis of $Ni(H_2BPZ)_3\cdot(CF_3SO_3)_2$ (9): $Ni(CF_3SO_3)_2\cdot(H_2O)_6$ (7.1 mg, 0.02 mmol) was dissolved in 2 mL of ethanol and mixed with H_2BPZ (6.4 mg, 0.05 mmol) in a glass tube which was closed with a plastic cap and then heated to 60 °C under solvothermal conditions for 3 days. The resulting light blue powder was filtered off and washed with ethanol. IR bands (cm^{-1}): 3301 (s), 3147 (w), 1674 (w), 1535 (w), 1467 (m), 1397 (m), 1314 (w), 1264 (s), 1242 (s), 1222 (s), 1161 (s), 1334 (s), 1049 (s), 1029 (s), 969 (m), 911 (s), 857 (s), 833 (m), 753 (w), 711 (s), 636 (s), 611 (s), 571 (s), 516 (s). Yield: 51%.

Synthesis of $Ni(H_2BPZ)_3\cdot(ClO_4)_2$ (10): $Ni(ClO_4)_2\cdot(H_2O)_6$ (55.4 mg, 0.15 mmol) was dissolved in 2 mL of ethanol and mixed with H_2BPZ (6.6 mg, 0.05 mmol) in a glass tube which was closed with a plastic cap and then heated to 70 °C under solvothermal conditions for 3 days. The resulting violet crystals were filtered off and washed with ethanol. IR bands (cm^{-1}): 3324 (br), 3134 (w), 1642 (w), 1537 (w), 1469 (m), 1391 (w), 1343 (m), 1257 (w), 1162 (m), 1130 (m), 1060 (s), 1037 (s), 1007 (s), 955 (w), 934 (s), 911 (s), 864 (m), 838 (m), 823 (m), 696 (m), 655 (m), 621 (s), 592 (m), 449 (s), 424 (w). Yield: 78%.

Synthesis of $Co(H_2BPZ)_3\cdot(ClO_4)_2$ (11): $Co(ClO_4)_2\cdot(H_2O)_6$ (37.2 mg, 0.10 mmol) was dissolved in 2 mL of ethanol and mixed with H_2BPZ (6.6 mg, 0.05 mmol) in a glass tube which was closed with a plastic cap and then heated to 90 °C under solvothermal conditions for 3 days. The resulting orange crystals were filtered off and washed with ethanol. IR bands (cm^{-1}): 3370 (br), 3134 (w), 1647 (w), 1540 (w), 1473 (m), 1393 (m), 1348 (m), 1260 (m), 1163 (m), 1137 (m), 1071 (s), 1039 (s), 1009 (s), 957 (m), 912 (m), 867 (m), 835 (m), 685 (m), 623 (s), 587 (m), 447 (m), 422 (w). Yield: 71%.

Synthesis of $Ni(BPZ)\cdot(DMF)_{0.65}$ (12): Hexakis(μ^2-3-phenyl-pyrazolato)trinickel(II) (9.1 mg, 0.01 mmol) was dissolved in 2 mL of DMF and mixed with H_2BPZ (16.0 mg, 0.12 mmol) dissolved in 2 mL and HCl (2 M, 500 μL) of DMF in a glass tube which was closed with a plastic cap and then heated to 120 °C under solvothermal conditions for 3 days. The resulting orange needles were filtered off and washed with DMF and ethanol. IR bands (cm^{-1}): 3121 (w), 1667 (s), 1507 (m), 1433 (w), 1398 (m), 1382 (m), 1273 (m), 1183 (m), 1164 (m), 1088 (m), 1060 (s), 919 (s), 819 (s), 658 (m), 635 (s), 461 (s), 410 (m). Yield: 65%.

Synthesis of Ni(BPZ) (13): Ni(BPZ) was obtained over different synthesis routes: (a) through activation of **12** at 200 °C under vacuum overnight, (b) through phase transition at elevated temperatures using **1**, **3**, **6**, **9**, and **12**, (c) direct synthesis: $Ni(ac)_2\cdot(H_2O)_6$ (29.9 mg, 0.12 mmol) was dissolved in 2 mL of water and mixed with H_2BPZ (6.8 mg, 0.05 mmol) in a glass tube which was closed with a plastic cap and then heated to 90 °C under solvothermal conditions for 3 days. IR bands (cm^{-1}): 1707 (w), 1511 (w), 1400 (m), 1355 (w), 1276 (m), 1187 (m), 1164 (m), 1062 (s), 921 (s), 820 (s), 669 (w), 633 (s), 528 (w), 465 (s), 417 (m). Yield: 58% (synthesis route c).

X-ray crystallographic data

Deposition Numbers 2113161 (for **1**), 2113162 (for **2**), 2113163 (for **5**), 2113164 (for **4**), 2113165 (for **7**), 2113166 (for **8**), 2113167 (for **3**), 2113168 (for **11**), 2113169 (for **10**), 2113110 (for **13**), 2113171 (for **12**), and 2113172 (for **9**) contain the supplementary crystallographic data for this paper. These data are provided free of charge by the joint Cambridge Crystallographic Data Centre and Fachinformationszentrum Karlsruhe Access Structures service www.ccdc.cam.ac.uk/structures.

Acknowledgements

The authors are grateful for financial support from DFG grant VO-829/12-2 (DFG Priority Program 1928 "Coordination Networks: Building Blocks for Functional Systems COORNETs)"). Open Access funding enabled and organized by Projekt DEAL.

Conflict of Interest

The authors declare no conflict of interest.

Keywords: Anions · Coordination polymers · Framework dimensionality · Phase transformation · Structure elucidation

[1] H. Furukawa, K. E. Cordova, M. O'Keeffe, O. M. Yaghi, *Science* **2013**, *341*, 1230444.
[2] a) M. Eddaoudi, J. Kim, N. Rosi, D. Vodak, J. Wachter, M. O'Keeffe, O. M. Yaghi, *Science* **2002**, *295*, 469; b) O. M. Yaghi, M. O'Keeffe, N. W. Ockwig, H. K. Chae, M. Eddaoudi, J. Kim, *Nature* **2003**, *423*, 705; c) Q. Yang, Q. Xu, H.-L. Jiang, *Chem. Soc. Rev.* **2017**, *46*, 4774.
[3] a) H. Hintz, S. Wuttke, *Chem. Commun.* **2014**, *50*, 11472; b) M. Kalaj, S. M. Cohen, *ACS Cent. Sci.* **2020**, *6*, 1046.
[4] K. S. Min, M. P. Suh, *J. Am. Chem. Soc.* **2000**, *122*, 6834.
[5] N. Stock, S. Biswas, *Chem. Rev.* **2012**, *112*, 933.
[6] R. Mondal, T. Basu, D. Sadhukhan, T. Chattopadhyay, M. k. Bhunia, *Cryst. Growth Des.* **2009**, *9*, 1095.
[7] E. V. Govor, A. B. Lysenko, E. B. Rusanov, A. N. Chernega, H. Krautscheid, K. V. Domasevitch, *Z. Anorg. Allg. Chem.* **2010**, *636*, 209.
[8] a) H.-M. Park, I.-H. Hwang, J.-M. Bae, Y.-D. Jo, C. Kim, H.-Y. Kim, Y.-M. Kim, S.-J. Kim, *Bull. Korean Chem. Soc.* **2012**, *33*, 1517; b) B. Notash, N. Safari, H. R. Khavasi, *CrystEngComm* **2012**, *14*, 6788.
[9] a) D. Zhao, D. J. Timmons, D. Yuan, H.-C. Zhou, *Acc. Chem. Res.* **2011**, *44*, 123; b) J. Lyu, X. Zhang, K.-I. Otake, X. Wang, P. Li, Z. Li, Z. Chen, Y. Zhang, M. C. Wasson, Y. Yang, P. Bai, X. Guo, T. Islamoglu, O. K. Farha, *Chem. Sci.* **2019**, *10*, 1186; c) M. Li, D. Li, M. O'Keeffe, O. M. Yaghi, *Chem. Rev.* **2014**, *114*, 1343; d) Y. Mu, Y. Ran, B. Zhang, J. Du, C. Jiang, J. Du, *Cryst. Growth Des.* **2020**, *20*, 6030.
[10] B. Liu, L. Wei, N. Li, W.-P. Wu, H. Miao, Y.-Y. Wang, Q.-Z. Shi, *Cryst. Growth Des.* **2014**, *14*, 1110.
[11] a) N. L. Toh, M. Nagarathinam, J. J. Vittal, *Angew. Chem.* **2005**, *117*, 2277; b) D. De, S. Neogi, P. K. Bharadwaj, *Cryst. Growth Des.* **2016**, *16*, 5238; c) Y.-P. Wu, D.-S. Li, F. Fu, W.-W. Dong, J. Zhao, K. Zou, Y.-Y. Wang, *Cryst. Growth Des.* **2011**, *11*, 3850; d) F. González Chávez, H. I. Beltrán, *New J. Chem.* **2021**, *45*, 6600.
[12] L.-F. Ma, L.-Y. Wang, D.-H. Lu, S. R. Batten, J.-G. Wang, *Cryst. Growth Des.* **2009**, *9*, 1741.
[13] a) S.-L. Li, K. Tan, Y.-Q. Lan, J.-S. Qin, M.-N. Li, D.-Y. Du, H.-Y. Zang, Z.-M. Su, *Cryst. Growth Des.* **2010**, *10*, 1699; b) C. Gabriel, M. Perikli, C. P. Raptopoulou, A. Terzis, V. Psycharis, C. Mateescu, T. Jakusch, T. Kiss, M. Bertmer, A. Salifoglou, *Inorg. Chem.* **2012**, *51*, 9282; c) W.-Q. Kan, J.-F. Ma, Y.-Y. Liu, H. Wu, J. Yang, *CrystEngComm* **2011**, *13*, 7037; d) I. Chi-Durán, J. Enríquez, C. Manquian, K. Wrighton-Araneda, W. Cañon-Mancisidor, D. Venegas-Yazigi, F. Herrera, D. P. Singh, *ACS Omega* **2018**, *3*, 801.
[14] a) A. Santra, P. K. Bharadwaj, *Cryst. Growth Des.* **2014**, *14*, 1476; b) M. J. Manos, E. E. Moushi, G. S. Papaefstathiou, A. J. Tasiopoulos, *Cryst. Growth Des.* **2012**, *12*, 5471; c) L. J. McCormick, S. A. Morris, A. M. Z. Slawin, S. J. Teat, R. E. Morris, *Cryst. Growth Des.* **2016**, *16*, 5771; d) B. Li, Q.-Q. Yan, G.-P. Yong, *Inorg. Chim. Acta* **2020**, *503*, 119403.
[15] a) Y.-B. Dong, Y.-Y. Jiang, J. Li, J.-P. Ma, F.-L. Liu, B. Tang, R.-Q. Huang, S. R. Batten, *J. Am. Chem. Soc.* **2007**, *129*, 4520; b) P. G. Derakhshandeh, S. Abednatanzi, K. Leus, J. Janczak, R. van Deun, P. van der Voort, K. van Hecke, *Cryst. Growth Des.* **2019**, *19*, 7096.
[16] P. Mahata, M. Prabu, S. Natarajan, *Inorg. Chem.* **2008**, *47*, 8451.
[17] A. D. Burrows, C. G. Frost, M. Kandiah, L. L. Keenan, M. F. Mahon, T. L. Savarese, J. E. Warren, *Inorg. Chim. Acta* **2011**, *366*, 303.

© 2021 The Authors. European Journal of Inorganic Chemistry published by Wiley-VCH GmbH

Research Article
doi.org/10.1002/ejic.202100853

[18] a) J. J. Mihaly, M. Zeller, D. T. Genna, *Cryst. Growth Des.* **2016**, *16*, 1550; b) Q. Fang, G. Zhu, M. Xue, Z. Wang, J. Sun, S. Qiu, *Cryst. Growth Des.* **2008**, *8*, 319.
[19] F.-M. Wang, L. Zhou, E. Velasco, J.-F. Li, X.-D. Xu, L.-Z. Chen, J. Li, *ACS Omega* **2021**, *6*, 16498.
[20] C. Pettinari, A. Tăbăcaru, I. Boldog, K. V. Domasevitch, S. Galli, N. Masciocchi, *Inorg. Chem.* **2012**, *51*, 5235.
[21] S. Spirkl, M. Grzywa, S. Reschke, J. K. H. Fischer, P. Sippel, S. Demeshko, H.-A. Krug von Nidda, D. Volkmer, *Inorg. Chem.* **2017**, *56*, 12337.
[22] S. Galli, N. Masciocchi, V. Colombo, A. Maspero, G. Palmisano, F. J. López-Garzón, M. Domingo-García, I. Fernández-Morales, E. Barea, J. A. R. Navarro, *Chem. Mater.* **2010**, *22*, 1664.
[23] V. A. Blatov, A. P. Shevchenko, *ToposPro*, TOPOS Expert, **2020**.
[24] D. Nicholls, B. A. Warburton, *J. Inorg. Nucl. Chem.* **1970**, 3871.
[25] N. A. Daugherty, J. H. Swisher, *Inorg. Chem.* **1968**, 1654–1653.
[26] J. Reedjik, *Recl. Trav. Chim. Pays-Bas* **1969**, 1451.
[27] M. J. Bagley, D. Nicholls, B. A. Warburton, *J. Chem. Soc. A* **1970**, 2694.
[28] T. Ishii, S. Tsuboi, G. Sakane, M. Yamashita, B. K. Breedlove, *Dalton Trans.* **2009**, 680.
[29] R. Tsuchida, *Bull. Chem. Soc. Jpn.* **1938**, *13*, 388.
[30] a) R. Díaz-Torres, S. Alvarez, *Dalton Trans.* **2011**, *40*, 10742; b) I. Anusiewicz, *J. Phys. Chem. A* **2009**, *113*, 11429.
[31] I. Boldog, J. Sieler, A. N. Chernega, K. V. Domasevitch, *Inorg. Chim. Acta* **2002**, *338*, 69.
[32] K. S. M. Salih, S. Bergner, H. Kelm, Y. Sun, A. Grün, Y. Schmitt, R. Schoch, M. Busch, N. Deibel, S. Bräse, B. Sarkar, M. Bauer, M. Gerhards, W. R. Thiel, *Eur. J. Inorg. Chem.* **2013**, *2013*, 6049.
[33] G. M. Sheldrick, *Acta Crystallogr. Sect. C* **2015**, *71*, 3.

Manuscript received: October 4, 2021
Revised manuscript received: December 1, 2021
Accepted manuscript online: December 3, 2021

© 2021 The Authors. European Journal of Inorganic Chemistry published by Wiley-VCH GmbH